Available online at www.sciencedirect.com
SCIENCE DIRECT
Journal of Solid State Chemistry 179 (2006) 2126–2132
JOURNAL OF SOLID STATE CHEMISTRY
www.elsevier.com/locate/jssc

Origin of stability of the high-temperature, low-pressure Rh_2O_3 III form of rhodium sesquioxide

Shuping Zhuo[a,b], Karl Sohlberg[b,*]

[a]School of Chemical Engineering, Shandong University of Technology, Zibo 255049, PR China
[b]Department of Chemistry, Drexel University, Philadelphia, PA 19104, USA

Received 23 December 2005; received in revised form 2 April 2006; accepted 5 April 2006
Available online 25 April 2006

Abstract

We present a first principles study of the equilibrium structures and relative thermodynamic stability of the three observed polymorphs of rhodium(III) sesquioxide. The thermodynamic Gibbs free energies for each phase are calculated as a function of P and T based on the electronic total energy, as well as vibrational energy and vibrational entropy contributions in the local harmonic (LH) approximation. The results confirm that Rh_2O_3 I is a low-temperature, low-pressure form and Rh_2O_3 II is a high-pressure form. A breakdown in the LH approximation at high T is then discussed and to address this breakdown an empirically corrected local harmonic (ECLH) approximation is introduced. ECLH demonstrates that the high-temperature, low-pressure form Rh_2O_3 III is entropically stabilized and produces a partitioning of phase space that is consistent with published experimental investigations.

Keywords: Rhodium sesquioxide; First-principles calculations; Structure; Phase transformation; Phase diagram; Free energy

1. Introduction

Rhodium as a metal has been used both in catalysts and electrochemical applications [1]. Rhodium supported on alumina has been the subject of numerous investigations because it is used in automotive catalytic converters to promote the reduction of NO [2–5]. In these cases, rhodium undertakes various redox reactions and consequently the role of rhodium is closely related to the formation of different polymorphs of Rh(III) oxide in different temperature ranges. Studies have shown that rhodium sesquioxides also exhibit the electrical and magnetic properties of a semiconductor [6,7]. Therefore, knowledge of the formation of Rh(III) oxide polymorphs, their structures and relative thermodynamic stability is important for understanding the nature of catalytic and electronic systems.

Several published experimental studies provide evidence for the existence of three polymorphs of Rh_2O_3. These are: the corundum form Rh_2O_3 I (space group R–3c) [8,9] described as the low-temperature, low-pressure form and two other corundum-related orthorhombic structures; the high-temperature, high-pressure form Rh_2O_3 II (space group *Pbna*) [10] and the high-temperature, low-pressure form Rh_2O_3 III (space group *Pbca*) [11–13]. So far, however, beyond these broad categorizations, the relative stabilities of the three phases are still unclear, and the P–T phase diagram for the three rhodium sesquioxide phases is basically unknown. To our knowledge, no theoretical work on phase transitions of the Rh(III) oxides has been reported in the literature.

In recent years, first-principles studies have been successfully used for predicting relatively complex solid-state phase diagrams for binary alloys by including the effects of lattice vibrations at finite temperatures [14,15]. The treatment of ionic solids is more rare [16]. First-principles techniques have also found application in the study of minerals that occur deep within the Earth's mantle, where pressures and temperatures exist that are not easily replicated in the laboratory [17,18]. In the present case, since characterization of the transitions to the high-pressure phase has not yet been assessed with experiments, first-principles theoretical studies can be of great help in

*Corresponding author. Fax: +1 215 895 1265.
E-mail address: sohlbergk@drexel.edu (K. Sohlberg).

0022-4596/$ - see front matter © 2006 Elsevier Inc. All rights reserved.
doi:10.1016/j.jssc.2006.04.015

understanding the relative stability of the three phases of rhodium sesquioxide over a range of temperatures and pressures [19].

In this paper, we investigate the relative thermodynamic stability of the three phases of Rh(III) oxide based on first-principles calculations including the contribution of lattice vibrations. The most elegant approach to including the effects of vibrations is to perform a numerically exact calculation of the phonon density of states (DOS) using linear-response theory [20–24]. Representative applications to ionic solids include Refs. [25–27]. Another numerically intensive technique is to apply quasiclassical lattice dynamics (QLD), which has been used to study SiO_2 at high pressures and temperatures [17]. In the present case, to construct the phase diagram, Gibbs free energies are computed from electronic total energies based on density-functional theory calculations (DFT) [28] and vibrational contributions to the free energy using the local harmonic (a.k.a. LH or Einstein-like) approximation [29,30]. The LH model is a very efficient technique for calculating free energies of solids [29,30]. It is especially useful when an exact calculation of the vibrational DOS is impractical or impossible. The LH approximation improves on the Einstein model in that the atomic vibrations are anisotropic and are explicitly dependent on the chemical environment. The LH approximation succeeds where the simple Debye model fails, and gives an exact prediction of the second moment of the vibrational DOS [29,30]. Vibrational frequencies for the LH model are from numerical second derivatives of the first-principles total energies with respect to spatial displacements of the atoms. To address certain shortcomings of the LH approximation at high T, an empirically corrected local harmonic (ECLH) approximation is introduced along with supporting analysis of the breakdown of the LH approximation at high T.

2. Theoretical methods

To construct the phase diagram for the three Rh_2O_3 phases, we calculate the Gibbs free energies,

$$G(T,P) = F(T,V) + PV \tag{1}$$

of each phase for different pressures and temperatures. The Helmholtz free energy F is calculated by

$$F(T,V) = E_e(V) + E_{vib}(T,V) - TS_{vib}. \tag{2}$$

Here $E_e(V)$ is the electronic total energy, and E_{vib} and S_{vib} are vibrational energy (including the zero-point energy) and vibrational entropy, respectively.

The theoretical calculations of the total energy $E_e(V)$ are based on density functional theory [28] employing the PW91 generalized gradient approximation (GGA) to the exchange-correlation energy [31,32], as described in the review by Payne et al. and coded in the Cambridge serial total energy package (CASTEP) [32]. The electron–ion interactions were described by the ultrasoft pseudopotentials of Vanderbilt [33]. We used a plane wave basis set with a cutoff energy 380 eV to construct the (valence) electronic wave functions. Here the valence consisted of oxygen 2*s* and 2*p* and Rh 5*s* and 4*d*. Integrations over the Brillouin zone employed a grid of k-points with a spacing of 0.1/Å chosen according to the Monkhorst–Pack scheme [34]. Convergence tests, as well as published work reporting plane-wave pseudopotential calculations on wide band-gap metal oxides, suggests that the total energy differences are converged with respect to the number of plane waves and k-point spacing to ca. 50–100 meV [35,36], and structural data to $<1\%$ [37,38].

To calculate the E_{vib} term, we have refined the Einstein model. In the Einstein model [39], the vibrational lattice energy $E_{vib}(T, V)$ of a pure metal is expressed in terms of a characteristic atomic local mode vibrational frequency v as

$$E_{vib}(T,V) = (3/2)hv + 3hv/(\exp((hv)/(kT)) - 1), \tag{3}$$

where h and k are the Plank and Boltzmann constants, respectively. For multi-element solid phase $Rh_{2n}O_{3n}$, we approximate $E_{vib}(T,V)$ by a modified Einstein model as follows:

$$\begin{aligned} E_{vib} = {} & 2n \sum_{i=1\ldots3} hv_{i\text{-Rh}}(1/2 + 1/(\exp(hv_{i\text{-Rh}}/kT) - 1)) \\ & + 2 \sum_{i=1\ldots3} hv_{i\text{-Oa}}(1/2 + 1/(\exp(hv_{i\text{-Oa}}/kT) - 1)) \\ & + n \sum_{i=1\ldots3} hv_{i\text{-Ob}}(1/2 + 1/(\exp(hv_{i\text{-Ob}}/kT) - 1)), \end{aligned} \tag{4}$$

where $v_{i\text{-Rh}}$ are the local mode vibrational frequencies for Rh and $v_{i\text{-Oa}}$ and $v_{i\text{-Ob}}$ are the vibrational frequencies for two types of oxygen atoms. The vibrational frequencies are computed in the harmonic approximation by diagonalizing the mass-weighted Cartesian force constant matrix for each symmetry unique atom in the primitive unit cell [40]. The Cartesian force constants are approximated by computing divided-difference numerical second derivatives of the electronic total energy (step size 0.01 Å).

Assuming that the crystal structure can be reasonably treated as a collection of harmonic oscillators, the vibrational entropy contribution S_{vib} can be expressed as [41,42]

$$\begin{aligned} S_{vib} = {} & -2nk \sum_{i=1\ldots3} \big(\ln[1 - \exp(-hv_{i\text{-Rh}}/kT)] \\ & - (hv_{i\text{-Rh}}/kT)[\exp(hv_{i\text{-Rh}}/kT) - 1]^{-1}\big) \\ & - 2nk \sum_{i=1\ldots3} \big(\ln[1 - \exp(-hv_{i\text{-Oa}}/kT)] \\ & - (hv_{i\text{-Oa}}/kT)[\exp(hv_{i\text{-Oa}}/kT) - 1]^{-1}\big) \\ & - nk \sum_{i=1\ldots3} \big(\ln[1 - \exp(-hv_{i\text{-Ob}}/kT)] \\ & - (hv_{i\text{-O}}/kT)[\exp(hv_{i\text{-Ob}}/kT) - 1]^{-1}\big). \end{aligned} \tag{5}$$

The dependence of total energy on volume was found by interpolation from a fourth degree polynomial fit to the DFT-calculated points on $E_e(V)$ for all V less than or equal

to the minimum energy volume. The isothermal dependencies $P(V)$ were calculated by direct differentiation of the energy, $P = -(\mathrm{d}E/\mathrm{d}V)_T$, for each structure. In this way, a specific pressure was related to a total energy, which was then used for E_e at that P for all T. Applying Eqs. (4) and (5) to Eqs. (1) and (2), Gibbs free energies for each phase can be obtained and used for constructing the phase diagram. To construct the phase diagram we recognize that at those points (P, T), where the difference between the Gibbs free energies of two phases is zero, both phases coexist. These points fall on curves of intersection between the free energy surfaces in the space where P and T are the independent variables.

It should be noted that the contribution of configurational entropy to the free energy is not included in Eq. (1). We assume that the configurational entropy of the Rh(III) oxide systems is mainly from the presence of oxygen vacancies. (The oxygen vacancy formation energy is lower than that of a rhodium vacancy.) We estimated the change in configurational entropy ΔS_{conf} introduced by the formation of an oxygen vacancy by [14,43]

$$\Delta S_{conf} = k(X_v \ln X_v + (1 - X_v) \ln(1 - X_v)), \quad (6)$$

where X_v is the vacancy concentration, which was in turn determined from first-principles total energy calculations of the vacancy formation energy ΔE_{vac} using Boltzmann statistics [43]. Based on the calculated oxygen vacancy formation energies for the three Rh_2O_3 phases (see Table 1), it was concluded that the configurational entropy differences between each pair of phases are sufficiently small to be justifiably neglected in constructing the phase diagram.

3. Results and discussion

The results of our calculations, including structural data and minimum total energies for Rh_2O_3 I, Rh_2O_3 II and Rh_2O_3 III are summarized in Table 1, along with published experimental results. The structures of these three forms are shown in Fig. 1.

That Rh_2O_3 I has the corundum structure was first determined by Lunde [8], whose lattice parameter data is included in Table 1, along with improved values reported by Coey [9]. Shannon and Prewitt [10] first reported the

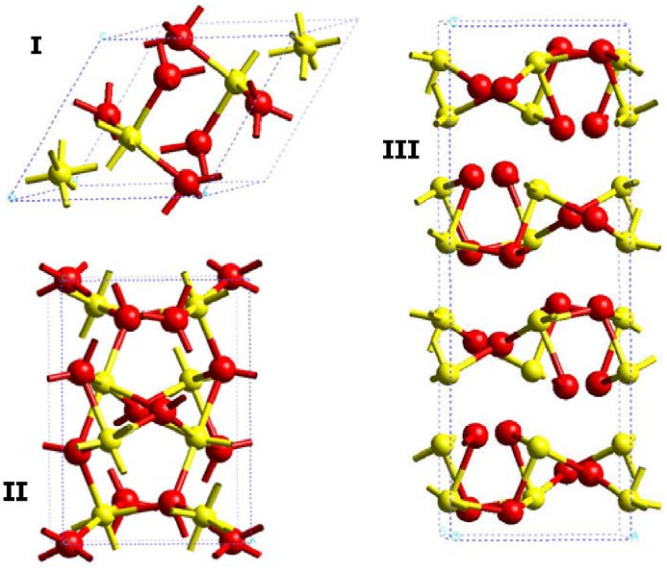

Fig. 1. Unit cell structures of the Rh_2O_3 I, II and III phases. Red = oxygen and yellow = rhodium.

Table 1
Calculated structural parameters and minimum energies of Rh_2O_3 I–III

	Lattice parameters		V (Å^3)	Density (g/cm^3)	E_e (eV)	$E_e + E_{vib}$ (eV)	ΔE_{vac} (eV)
	Theo. (Å)	Exp. (Å)					
Rh_2O_3 I	$a = 5.601$	$a = 5.47$[a] ($a = 5.485$[b])	111.38	7.57	−20,277.30	−20,261.03	3.4
($R-3c$)	$\alpha = 55.54°$	$\alpha = 55.67$[a] ($\alpha = 55.73$[b])	(445.52)				
($Z = 2$)							
Rh_2O_3 II	$a = 5.257$	5.1686[c]	212.69	7.93	−20,277.07	−20,260.77	3.3
($Pbna$)	$b = 5.481$	5.3814[c]	(425.38)	(8.26[d])			
($Z = 4$)	$c = 7.382$	7.2426[c]					
Rh_2O_3 III	$a = 5.236$	5.149[d] (5.1477[e], 5.146[f])	435.70	7.76	−20,277.18	−20,260.48	3.6
($Pbca$)	$b = 5.538$	5.436[d] (5.4425[e], 5.440[f])		(8.06[d])			
($Z = 8$)	$c = 14.994$	14.688[d] (14.6977[e], 14.71[f])					

Energies are given in eV per $Rh_{16}O_{24}$ unit. (The $Z = 8$ supercell volume is given in parenthesis in the column labeled "V". Other values in parenthesis are from the sources cited.)

[a]From Ref. [8].
[b]From Ref. [9].
[c]From Ref. [10].
[d]From Ref. [11].
[e]From Ref. [12].
[f]From Ref. [6].

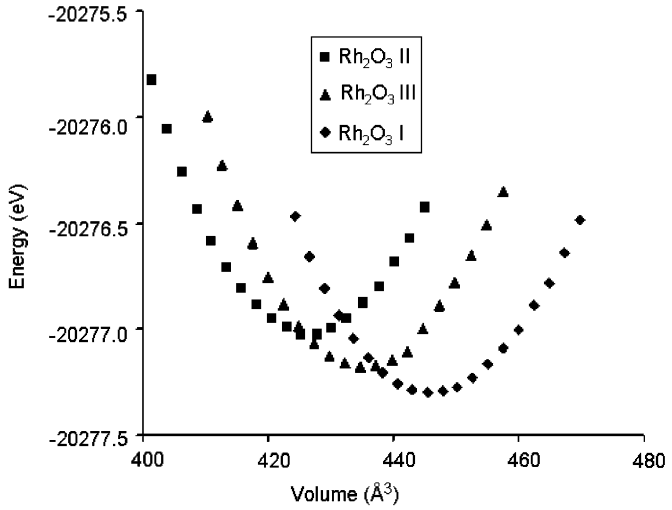

Fig. 2. Energy versus volume curves of the Rh_2O_3 I, II and III phases.

synthesis and characterization of Rh_2O_3 II, an orthorhombic corundum-related form. Rh_2O_3 III also has an orthorhombic structure. Lattice parameters by Wold et al. [11], Biesterbos and Hornstra [12], and Leiva et al. [6] are collected in Table 1.

It has been suggested that Rh_2O_3 III is in some respects an intermediate form between the other two types [13]. Comparing both the present results and the previous experimental results given in Table 1, it is interesting to note that the material density of Rh_2O_3 III is indeed "intermediate" between Rh_2O_3 I and Rh_2O_3 II. The variation in the total energy with volume for each of the three phases is shown in Fig. 2. Rh_2O_3 III also shows this "intermediate" property in the $E_e(V)$ curves.

3.1. Total energy as a function of volume for the three Rh_2O_3 phases at $T = 0$ K

From the total energy curves it can be seen that the three phases have very similar total energies at their minima. Rh_2O_3 I has the lowest total energy minimum. The minima of the total energies for the Rh_2O_3 II and Rh_2O_3 III structures lie 0.23 and 0.12 eV above that of Rh_2O_3 I (per $Rh_{16}O_{24}$ unit). These energy differences are very small and are near the limit of accuracy of the total energy calculations so that no definitive conclusion can be drawn from the calculated relative order in energy, $E_e(Rh_2O_3\ I) < E_e(Rh_2O_3\ III) < E_e(Rh_2O_3\ II)$. Lending credibility to the observed energetic preference for Rh_2O_3 I, however, we found that when E_e is corrected for zero-point vibrational energy ($E_z = E_e + E_{vib}(T = 0)$) Rh_2O_3 I is still the most stable phase at 0 K (see Table 1).

The total energy curves shown in Fig. 2 suggest that Rh_2O_3 undergoes a series of structural phase transitions under increasing pressure. The sequence of the structural phase transitions is: Rh_2O_3 I → Rh_2O_3 III → Rh_2O_3 II. We may use the total energy curves in Fig. 2 obtained by DFT calculations to estimate the zero-temperature phase transition pressures. According to the equation $P = -(dE/dV)_T$, the transition pressures are 1.8 and 2.6 GPa for Rh_2O_3 I → Rh_2O_3 III and Rh_2O_3 III → Rh_2O_3 II, respectively. For the direct phase transition from Rh_2O_3 I to Rh_2O_3 II at 0 K, the transition pressure is 2.2 GPa. These are coarse theoretical estimates because they neglect ZPE, but it seems reasonable to conclude that there is at most a small pressure range for the existence of Rh_2O_3 III at low T. No other experimental or theoretical results are available for comparison with these estimates of the transition pressure at 0 K, but we refine our analysis in the following sections.

3.2. P–T phase diagram in the LH approximation

In order to consider the phase transitions at finite temperatures, it is necessary to consider the vibrational contributions to the free energy in evaluating the relative stability of each pair of phases. Lattice vibrations can have significant influence on predictions of phase stability [14,30]. To construct the phase diagram, the thermodynamical Gibbs potentials $G(P,T)$, including the vibrational entropy contribution, were calculated according to Eq. (1) and then compared for the three phases on a fixed mesh of independent parameters (P, T).

To construct the P–T diagram we have first applied the LH model for vibrational contributions to the free energy. For a given crystal structure at a volume V, one can determine the vibrational frequencies in the LH approximation v_i by diagonalizing the local dynamical matrix for each independent atom in the unit cell (i.e. by diagonalizing the 3×3 block-diagonal approximation to the force constant matrix $\boldsymbol{F}$). These local-mode frequencies, inserted into Eqs. (4) and (5), yield the E_{vib} and S_{vib} terms, which enter into the thermodynamic quantities $F(T,V)$ and $G(T,P)$. By comparing the relative values of $G(T,P)$ for the three Rh_2O_3 phases, the P–T phase diagram is constructed and presented in Fig. 3.

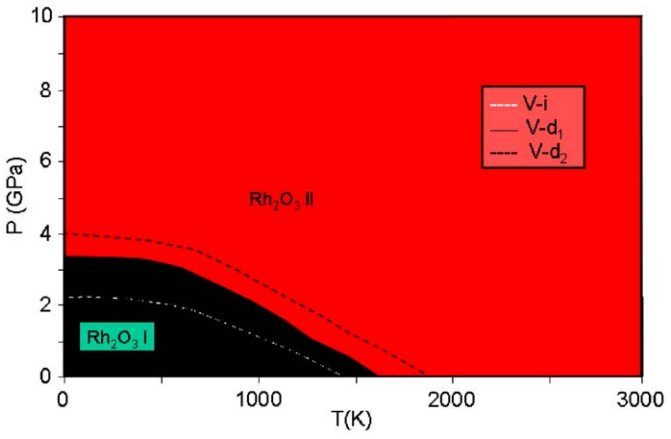

Fig. 3. Phase diagram for Rh(III) oxides from first-principles in the LH approximation. The three placements of the phase boundary show its sensitivity with respect to variation of the computed local-mode vibrational frequencies. The solid curve is recommended.

Fig. 3 shows three placements of the Rh_2O_3 I/II phase boundary calculated using the LH approximation. First, we computed the local-mode vibrational frequencies for the Rh and O atoms at the minimum-energy volume for each of three Rh_2O_3 phases and assumed these frequencies to be volume independent. This produced the phase boundary indicated by the white dashed line in the black area (V-i in Fig. 3). Next, to obtain the volume dependence of the vibrational frequencies, we computed the vibrational frequencies explicitly from first principles at several volumes and derived a linear dependence for each $v_i(V)$ based on least-squares fitting. These volume-dependent frequencies produced the solid line dividing the black and red regions in the P–T phase diagram (V-d_1 in Fig. 3). Third, to further estimate the sensitivity of the P–T diagram to the computed frequencies we excluded those vibrations exhibiting the greatest deviations from a linear volume dependence (Rh_2O_3 II data at the volume displaying the most negative deviation; Rh_2O_3 III data at the volume displaying the most positive deviation) and obtained the phase boundary depicted by the black dashed line in the red region (V-d_2 in Fig. 3). The sensitivity of the phase boundaries to the frequencies is thereby exhibited in the P–T phase diagram. It is notable that all three of these calculations give a similar shape of the stability region for Rh_2O_3 I. They do not, however, produce a region of stability for the Rh_2O_3 III form in the entire P–T range shown for reasons discussed in Section 3.3. In the remainder of this subsection, our "recommended" results, denoted by the solid line in Fig. 3, are used.

There is also likely to be some error in the vibrational frequencies arising from the choice of the GGA functional. The mean absolute relative error in the lattice parameters is 1.9%, so we can expect errors of at least this magnitude in the computed frequencies. Errors of this magnitude are minor on the scale of the sensitivity analysis presented in the previous paragraph, and are well below the anticipated error due to neglecting anharmonicity in the vibrations (ca. 5%), suggesting that GGA is adequate.

From the phase boundary between Rh_2O_3 I and II in Fig. 3, it is clear that the transition between Rh_2O_3 I and Rh_2O_3 II occurs in the temperature range $T < 1630$ K and the pressure range 0.0–3.27 GPa, which is consistent with experimental observations that Rh_2O_3 II has been obtained by heating rhodium oxide at 1200–1500 °C under 65 kbar (6.5 GPa) pressure [6,10]. (Since the experimental condition was in air, only qualitative comparison is possible.) Fig. 4 focuses on a representative point of intersection between the free energy surfaces for the Rh_2O_3 phases at $P = 1.0$ GPa, which shows that over the range $0 < T < 1270$ K, the Gibbs free energy is lowest in the Rh_2O_3 I phase; while for $T > 1270$ K, the Rh_2O_3 II phase becomes preferred. The point of the intersection of the curves lies on the phase boundary between Rh_2O_3 I and Rh_2O_3 II of the P–T diagram in Fig. 3. The P–T diagram shows, in agreement with experimental results, that Rh_2O_3 I is the low-temperature, low-pressure form, while Rh_2O_3 II is the high-pressure form. In the LH approximation, however, the Rh_2O_3 III form is never thermodynamically favored in the region of P, T space studied here.

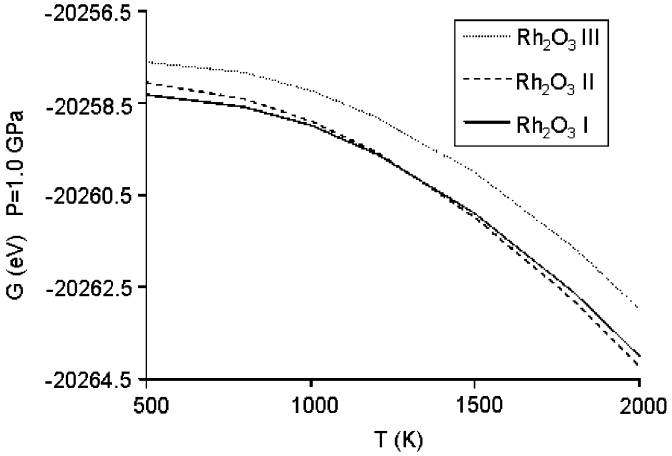

Fig. 4. The temperature dependence of the Gibbs energy at $P = 1.0$ GPa.

3.3. P–T phase diagram in the ECLH approximation

In this section, we explore why the LH approximation fails to produce a region of stability for the Rh_2O_3 III phase. As has been pointed out [30], the LH approximation neglects coupling off the 3×3 diagonal block of the force constant matrix $\boldsymbol{F}$. This approximation has little impact on high frequency vibrations. High frequency phonon modes generally result from local oscillations of single atoms. (Nominally frequency is proportional to mass$^{-1/2}$ so that the highest frequencies correspond to moving the smallest possible masses, i.e. individual atoms.) Since these high frequency modes are weakly coupled, they are adequately approximated using only the 3×3 block-diagonal (LH) approximation to $\boldsymbol{F}$. They are also accurately captured when a small unit cell is used to model the material. The major contribution to the vibrational energy E_{vib} comes from the intermediate and high frequencies of the phonon spectrum [30] and high frequency vibrations dominate the zero-point-energy (ZPE) term. Calculations of the free energy G based on small unit cells and the LH approximation are therefore expected to be reliable at low T where $TS_{vib} \approx 0$ and $E_{vib} \approx$ ZPE. At high T, however, TS_{vib} is appreciable and this term is dominated by low frequency vibrations. (Very-low, i.e. near-zero, frequency vibrations carry so little energy that they are of little consequence except at temperatures not customarily relevant.) Low frequencies arise from groups of atoms oscillating together, and such oscillations are not captured by a small unit cell. In addition, since low frequency modes involve the interaction of multiple atoms, they are not accurately modeled with the LH approximation. From the preceding discussion we can conclude that the P–T phase diagram based on the LH approximation will not be reliable at high T.

To accurately capture low-frequency oscillations, we must avoid small unit cells and avoid the LH approximation. Let us estimate the computational expense of going beyond the LH approximation within the present theoretical framework: to obtain the vibrational frequencies we must diagonalize the force constant matrix $\boldsymbol{F}$. Each element of $\boldsymbol{F}$ is proportional to a second derivative of the total energy E_e. $F_{ij} \propto \partial^2 E_e/\partial q_i \partial q_j = (m_1^{-1/2} m_2^{-1/2}) \partial^2 E_e/\partial q_i \partial q_j$, where q_i and q_j are spatial coordinates and m_1 and m_2 are the corresponding atomic masses. For Rh_2O_3 I, which has 10 atoms in the primitive unit cell, $\boldsymbol{F}$ has dimension 30×30. Taking advantage of the fact that $\boldsymbol{F}$ is symmetric about the diagonal, $(30^2 + 30)/2 = 465$ second derivatives of the total energy must be computed. For Rh_2O_3 II, which has a 20-atom unit cell, the number of unique $\boldsymbol{F}$ matrix elements is $(60^2 + 60)/2 = 1830$ and for Rh_2O_3 III the number is $(120^2 + 120)/2 = 7260$. Moreover, if full diagonalization of $\boldsymbol{F}$ is carried out for III, to properly compare E_{vib} and S_{vib} between phases, we must use the $z = 8$ supercell for I and for II also. The above discussion neglects volume dependence. If we want to include volume dependence, we would need to construct each $\boldsymbol{F}$ at several volumes, resulting in numerous $\boldsymbol{F}$ matrices each with dimensions 120×120, a computationally prohibitive calculation.

It seems reasonable to conclude that the highest frequencies resulting from the LH approximation are reliable, but the low frequencies are not reliable because of the neglect of coupling and because the smallest possible unit cells were used. We turn to Ref. [13], which reports infrared (IR) spectra below 700 cm^{-1} for Rh_2O_3 I, II and III. We can use this experimental data to carry out an empirical correction to the LH approximation (ECLH). Since Ref. [13] tabulates four or more low frequencies for each polymorph, we may replace the lowest four frequencies found with the LH model by the lowest four experimental frequencies. (We normalize to the Rh_2O_3 formula unit so that 4/15 of the frequencies are replaced for each phase.) In other words, the four lowest theoretical frequencies (presumably the *least reliable* theoretical frequencies owing to the neglect of coupling in the LH approximation) are dropped and replaced with experimental data. Replacing the low frequencies will have very little effect on the zero point energy, since it is dominated by high frequencies. The P–T diagram at low T will change very little. At high T, the P–T diagram will change appreciably because low frequencies contribute heavily to TS_{vib}. Fig. 5 shows the P–T phase diagram resulting from the ECLH approximation.

As shown in Fig. 5, the ECLH calculation gives a high temperature, low-pressure region of stability for the Rh_2O_3 III form, which is in agreement with the experimental result that the corundum structure Rh_2O_3 I transforms irreversibly to Rh_2O_3 III when heated between 750 and 1000 °C in the air [6]. As expected, the P–T diagram at low T changes very little from that obtained with the LH model, which confirms that Rh_2O_3 I is the low-pressure, low-temperature form and Rh_2O_3 II remains a high-pressure form. We

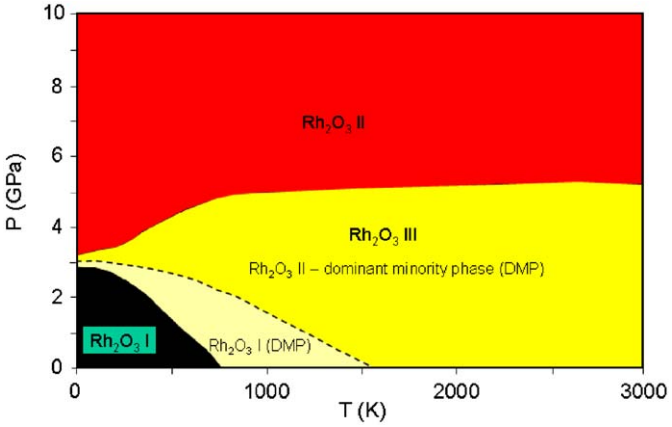

Fig. 5. Phase diagram for Rh(III) oxides in the ECLH approximation. Note that the phase boundary for the Rh_2O_3 I → Rh_2O_3 II transformation is in good agreement with that predicted with the LH approximation. The empirical correction introduces a region of stability for the Rh_2O_3 III form at high T and low P, in agreement with published experimental results; although we suggest that the diagram should be accepted as semi-quantitative for reasons discussed in the text.

presume that the P–T diagram is only qualitatively corrected by the empirical frequency data, which predicts that Rh_2O_3 III is favored at high temperature and becomes the majority phase. To more accurately and quantitatively map the region of stability for the Rh_2O_3 III phase, we should go beyond the LH approximation completely, which will not be considered in this paper owing to the aforementioned prohibitive computational expense. The present calculations, however, do show clearly that the Rh_2O_3 III phase is intermediate between Rh_2O_3 I and Rh_2O_3 II and is stabilized by vibrational entropy.

4. Summary

Using first-principles total energy calculations, we have investigated the structures and relative phase stability of the three rhodium sesquioxides Rh_2O_3 (I, II, III). The P–T phase diagram when constructed with the LH approximation identifies regions of thermodynamic stability for the Rh_2O_3 I and Rh_2O_3 II phases, and shows that Rh_2O_3 I is a low-temperature, low-pressure form while Rh_2O_3 II phase is a high-pressure phase. Using the LH approximation, Rh_2O_3 III is never thermodynamically favored in the P, T region studied here. We then analyze why low-frequency vibrational modes are less reliably predicted than high frequency modes when using the LH approximation. An ECLH approximation is introduced in which the less reliable low-frequencies from the LH approximation are replaced with experimental data. The ECLH calculation produces a region of stability at high-temperature and low-pressure for the Rh_2O_3 III form. The $G(T, P)$ results yield qualitative relative phase stabilities that are in agreement with inferences about the regions of stability from previous experimental reports and demonstrate that Rh_2O_3 III is entropically stabilized. We anticipate that this new insight

into the Rh(III) oxides will be helpful to understand the role of these oxides in processes on supported rhodium catalysts.

Acknowledgments

This research was sponsored by the US Department of Energy under Contract no. DE-FC02-01CH11085, by National Science Foundation GOALI Grant no. DMR-0111841 with Alcoa Inc., and by a DuPont Young Professor award to KS, who also thanks Prof. R. Schweitzer-Stenner for useful discussions of the LH model.

References

[1] A. Saric, S. Popovic, R. Trojko, S. Music, J. Alloys Compounds 320 (2001) 140.
[2] P.D. Nellist, S.J. Pennycook, Science 274 (1996) 413.
[3] L.A. Carol, G.S. Mann, Oxid. Met. 34 (1990) 1.
[4] Z. Weng-Sieh, R. Gronsky, A.T. Bell, J. Catal. 170 (1997) 62.
[5] Z. Weng-Sieh, R. Gronsky, A.T. Bell, J. Catal. 174 (1998) 22.
[6] H. Leiva, R. Kershaw, K. Dwight, A. Wold, Mater. Res. Bull. 17 (1982) 1539.
[7] A. Roy, J. Ghose, Mater. Res. Bull. 33 (1998) 547.
[8] G. Lunde, Z. Anorg. Allg. Chem. 163 (1927) 345.
[9] J.M.D. Coey, Acta Crystallogr. B B26 (1970) 1876.
[10] R.D. Shannon, C.T. Prewitt, J. Solid State Chem. 2 (1970) 134.
[11] A. Wold, R.J. Arnott, W.J. Croft, Inorg. Chem. 2 (1963) 972.
[12] J.W.M. Biesterbos, J. Hornstra, J. Less-Common Met. 30 (1973) 121.
[13] K.R. Poeppelmeier, J.M. Newsam, J.M. Brown, J. Solid State Chem. 60 (1985) 68.
[14] A.v.d. Walle, G. Ceder, Rev. Mod. Phys. 74 (2002) 11.
[15] A.v.d. Walle, G. Ceder, U.V. Waghmare, Phys. Rev. Lett. 80 (1998) 4911.
[16] G. Ceder, A. Van der Ven, C. Marianetti, D. Morgan, Model. Simul. Mater. Sci. Eng. 8 (2000) 311.
[17] A.R. Oganov, M.J. Gillan, G.D. Price, J. Chem. Phys. 118 (2003) 10174.
[18] C.S. Zha, H.K. Mao, R.J. Hemley, in: Proceedings of the National Academy of Sciences of the United States of America, 2000, p. 13494.
[19] D.D. Klug, R. Rousseau, K. Uehara, M. Bernasconi, Y.L. Page, J.S. Tse, Phys. Rev. B 63 (2001) 104106.
[20] S. Baroni, P. Giannozzi, Phys. Rev. Lett. 58 (1987) 1861.
[21] S.Y. Savrasov, Phys. Rev. Lett. 69 (1992) 2819.
[22] R. Yu, H. Krakauer, Phys. Rev. B 49 (1994) 4467.
[23] P. Giannozzi, S.D. Gironcoli, Phys. Rev. B 43 (1991) 7231.
[24] P. Pavone, K. Karch, O. Schutt, W. Windl, D. Strauch, Phys. Rev. B 48 (1993) 3156.
[25] J.M. An, H. Rosner, S.Y. Savrasov, W.E. Pickett, Physica B 328 (2003) 1.
[26] M. Verstraete, X. Gonze, Phys. Rev. B (2003) 195123.
[27] N. Choudhury, Z. Wu, E.J. Walter, R.E. Cohen, Phys. Rev. B (2005) 125134.
[28] W. Kohn, L.J. Sham, Phys. Rev. 140 (1965) 1133.
[29] R. LeSar, R. Najafabadi, D.J. Srolovitz, Phys. Rev. Lett. 63 (1989) 624.
[30] G.D. Garbulsky, G. Ceder, Phys. Rev. B 53 (1996) 8993.
[31] J.P. Perdew, Phys. Rev. B 33 (1986) 8822.
[32] J.P. Perdew, Y. Wang, Phys. Rev. B 45 (1992) 13244.
[33] D. Vanderbilt, Phys. Rev. B 41 (1990) 7892.
[34] H.J. Monkhorst, J.D. Pack, Phys. Rev. B 13 (1976) 5188.
[35] G. Kresse, W. Bergermayer, R. Podloucky, E. Lundgren, R. Koller, M. Schmid, P. Varga, Appl. Phys. A 76 (2003) 701.
[36] D.R. Jennison, A. Bogicevic, Faraday Discuss. 114 (1999) 45.
[37] B. Meyer, J. Padilla, D. Vanderbilt, Faraday Discuss. 114 (2000) 395.
[38] I.G. Batyrev, A. Alavi, M.W. Finnis, Phys. Rev. B 62 (2000) 4698.
[39] R. Kubo, T. Nagamiya, Solid State Physics, McGraw-Hill Book Co., Inc., New York, 1969.
[40] S. Califano, Vibrational States, Wiley, London, 1976.
[41] M. Born, K. Huang, Dynamical Theory of Crystal Lattices, Oxford University Press, London, 1954.
[42] H.B. Huntington, G.A. Shirn, E.S. Wajda, Phys. Rev. B 99 (1955) 1085 (There appears to be a misprint in equation 5 of this widely cited reference. A survey of the literature suggests that no papers by its authors or other authors have reported this error. Equation 16.11 of reference 39 is used herein.).
[43] A. Green, J. Humphreys, R. Mackenzie, Introduction to point defects, 1997. http://www.matter.org.uk/matscicdrom/manual/po.html